Damping of Antiferromagnetic Spin Waves by Valence Fluctuations in the Double Layer Perovskite YBaFe$_2$O$_5$

S. Chang,[1,*] P. Karen,[2] M. P. Hehlen,[3] F. R. Trouw,[3] and R. J. McQueeney[1,4]

[1]*Ames Laboratory, Ames, Iowa 50011, USA*
[2]*Department of Chemistry, University of Oslo, N-0315 Oslo, Norway*
[3]*LANSCE, Los Alamos National Laboratory, Los Alamos, New Mexico 87545, USA*
[4]*Department of Physics and Astronomy, Iowa State University, Ames, Iowa 50011, USA*
(Received 7 February 2007; published 19 July 2007)

Inelastic neutron scattering experiments show that spin dynamics in the charge-ordered insulating ground state of the double layer perovskite YBaFe$_2$O$_5$ is well described in terms of e_g superexchange interactions. Above the Verwey transition at $T_V = 308$ K, t_{2g} double exchange-type conduction proceeds within antiferromagnetic FeO$_2$-BaO-FeO$_2$ double layers by an electron hopping process that requires a spin flip of the five-coordinated Fe ions, costing an energy of $5\langle J \rangle S^2 \approx 0.1$ eV. The hopping process disrupts near-neighbor spin correlations, leading to massive damping of zone-boundary spin waves.

The extraordinary electrical transport properties of strongly correlated transition-metal oxides are often intimately related to magnetic interactions. For example, in the doped perovskite manganites, electron spins in the itinerant e_g band are aligned parallel to the localized t_{2g} spins due to strong Hund's rule coupling. Thus, conduction of spin-polarized e_g electrons results in ferromagnetic (F) nearest-neighbor interactions, known as double exchange (DE) [1]. However, antiferromagnetic (AF) superexchange (SE) via localized t_{2g} electrons, cooperative Jahn-Teller distortions, as well as on site and intersite Coulomb repulsion may compete with DE leading to different insulating magnetic-, orbital-, or charge-ordered phases [2]. RBaFe$_2$O$_5$ ($R =$ Nd–Ho and Y) [3] double layer perovskites are another class of compounds where DE and SE interactions are in competition, resulting in either a charge-ordered insulator or a valence-mixed conducting phase [4,5]. However, in RBaFe$_2$O$_5$, DE occurs via the minority spin t_{2g} electrons in competition with AF SE dominated by the e_g bands. Both SE and DE may be modified in the charge- or orbital-ordered ground state due to structural distortions and the fractional d_{xz} orbital occupancy at the metal site [4]. Therefore, spin excitations provide a window into the underlying charge dynamics. In this Letter, we report on an inelastic neutron scattering study of the magnetic excitations in YBaFe$_2$O$_5$. The charge-ordered insulating ground state below the Verwey temperature T_V can be well understood in terms of normal SE interactions. However, above T_V, strong coupling with valence fluctuations leads to massive damping of the zone-boundary spin waves.

YBaFe$_2$O$_5$ is a fractional valent material with the Fe atoms possessing a nominal valence of 2.5+. The perovskite-based crystal structure of YBaFe$_2$O$_5$ consists of FeO$_2$-BaO-FeO$_2$ double layers, in which five-coordinated Fe sites form apex-shared square pyramids. The double layers are separated by an oxygen-vacant Y

layer. At high temperatures, YBaFe$_2$O$_5$ is valence-mixed and paramagnetic. On cooling, the compound orders antiferromagnetically at $T_N = 432$ K [6] but remains valence-mixed. At $T_V = 308$ K, a Verwey-type transition orders the Fe valences in real space and modifies the AF structure. The magnetic- and charge-ordering patterns [4] for $T < T_V$ (AF$_{CO}$) and $T_V < T < T_N$ (AF$_{VM}$) are shown in Fig. 1. Both AF$_{CO}$ and AF$_{VM}$ structures are characterized by strong AF coupling of Fe atoms within double layers due
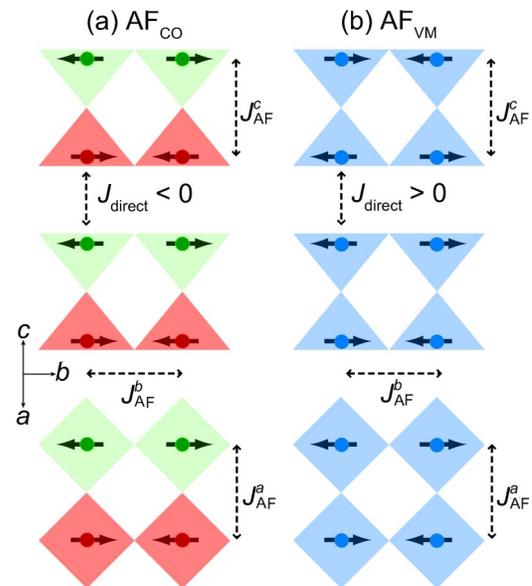

FIG. 1 (color online). Schematic representations of charge and magnetic order [4] in YBaFe$_2$O$_5$. The upper and lower panels are projections onto the bc and ab planes, respectively. Fe ions are shown as balls and oxygen square pyramids as triangles or squares. Arrows indicate magnetic moments. (a) For $T < 308$ K (AF$_{CO}$), Fe^{2+} (green online) and Fe^{3+} (red online) chains run along the b axis and alternate along the a and c directions. (b) For 308 K $< T <$ 430 K (AF$_{VM}$), the Fe ions are valence-mixed (blue online).

to e_g SE interactions through nearly 180° Fe-O-Fe bonds. The main difference between the two AF structures is the sign of the direct exchange between double layers (across the Y layer): F in AF_{VM} and AF in AF_{CO}. However, this direct exchange is much weaker than AF SE within double layers due to the large Fe-Fe interlayer distance (∼3.6 Å [4]). This is shown by using perturbation theory to estimate the ratio of direct exchange (J_{direct}) and SE (J_{AF}) for a linear Fe-Fe bond [7]

$$\frac{J_{direct}}{J_{AF}} \propto \frac{t_{dd}^2/U}{t_{pd}^4/\Delta^3} \approx \frac{m^2}{\hbar^4} \frac{\Delta^3}{U} \frac{\eta_{dd\sigma}^2}{\eta_{pd\sigma}^4} \frac{d_{Fe-O}^{14}}{d_{Fe-Fe}^{10}} = 1\%, \quad (1)$$

where t_{pd} and t_{dd} are the Fe-O and Fe-Fe overlap integrals, respectively, U is the on site Coulomb repulsion, and Δ is the charge transfer energy. These parameters are estimated as $U = 8$ eV and $\Delta = 3$ eV [8]. Overlap integrals are estimated using Harrison's method [9] with $d_{Fe-Fe} = 3.6$ Å, $d_{Fe-O} = 2.0$ Å [4], and the coefficients of the radial overlap integrals are $\eta_{dd\sigma} = 16.2$ and $\eta_{dp\sigma} = 2.95$ [9]. Furthermore, due to the layered crystal structure, charge fluctuations through the direct Fe-Fe bond alone cannot provide a continuous path for conduction in the valence-mixed AF_{VM} phase.

To study the spin waves, we performed time-of-flight (TOF) powder inelastic neutron scattering measurements on approximately 50 g of $YBaFe_2O_5$ using the Pharos spectrometer at the Lujan Center, Los Alamos National Laboratory. The master sample of $YBaFe_2O_5$ was synthesized in several batches from citrate precursors as reported in Ref. [4]. The combined batches were equilibrated at 400 °C for 33 days in a sealed silica ampoule together with 0.03 g Zr foil as a getter, placed 12 cm from the sample, and locally heated to 700 °C. This was followed by a cooldown at a rate of 0.1 °C/min. The oxygen content, determined by cerimetric titration, was 5.005(1) per formula at the top of this batch and 5.003(1) at the bottom. The sample quality was verified by x-ray powder diffraction, differential scanning calorimetry, and magnetization measurements, which were in good agreement with previous results [4]. The powder was loaded in a flat aluminum can and mounted on the cold head of a closed-cycle He cryostat. For temperatures greater than 325 K, a displex with a high-temperature stage was used. The sample was oriented at 45° to the incident neutron beam, and inelastic neutron spectra were measured at various temperatures between 6 and 450 K, with an incident energy $E_i = 120$ meV. The TOF data were corrected for energy-dependent detector efficiencies and instrumental background and reduced into energy transfer (E) and scattering angle (2θ) histograms. The resulting spectra contain both magnetic and phonon contributions. However, since the magnetic intensity disappears at high angles due to the magnetic form factor, it is possible to segregate the magnetic and phonon scattering by summing the data over different angle ranges. For the present experiment, we chose angle ranges $2\theta = 1°–35°$ and $55°–95°$ for low

(magnetic) and high (phonon) angle data, respectively. The phonon contribution to the scattered intensity in the low angle data was removed by subtracting the appropriately scaled high angle data.

The total scattered intensity for $YBaFe_2O_5$ at 6 K in the charge-ordered AF_{CO} phase is shown as a function of Q (the magnitude of momentum transfer vector **Q**) and E in Fig. 2(a). The main feature in the spectrum in the angle range $1°–35°$ is a prominent band of scattering between 50–65 meV arising from zone-boundary spin waves. The band appears as two (or more) overlapping peaks in the phonon-subtracted magnetic intensity shown in Fig. 2(c). Additional weak features below 40 meV are due to imperfect subtraction of phonon bands near 20 and 40 meV as well as dispersive features from both spin waves and phonons appearing as vertical streaks in Fig. 2(a).

Measurements of polycrystalline-averaged spin excitation spectra of long-range magnetically ordered material result in neutron scattering intensities related to the spin-wave density of states (SWDOS). Below T_V, the SWDOS of insulating and charge-ordered $YBaFe_2O_5$ may be understood by considering only SE interactions [7] within
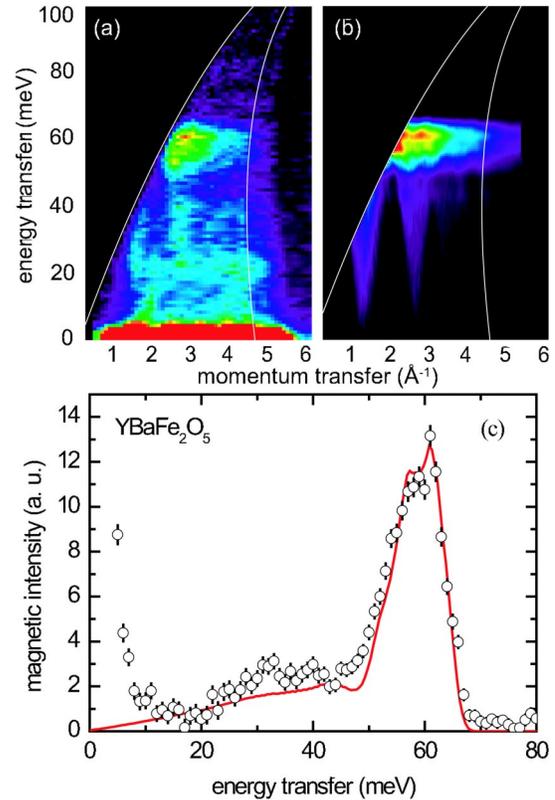

FIG. 2 (color online). (a) Inelastic neutron scattering intensity $S(Q, E)$ for $YBaFe_2O_5$ at $T = 6$ K. White lines are loci of constant angles in (Q, E) space that denote limits of the angle summation $2\theta = 1°–35°$. (b) Calculation of $S(Q, E)$ for $YBaFe_2O_5$ at $T = 6$ K using a Heisenberg model with $J_{33} = 5.9$ meV, $J_{22} = 3.4$ meV, and $J_{23} = 6.0$ meV. (c) Comparison of angle-summed magnetic scattering data (open symbols) with Heisenberg model calculation (line).

double layers and is comparable to the *G*-type AF perovskite LaFeO$_3$ (see Fig. 3). LaFeO$_3$ may be considered isotropic with a single nearest-neighbor exchange constant $J_0 \approx 5$ meV and spin $S = 5/2$ [10]. The SWDOS of LaFeO$_3$ consists of a single sharp peak indicating a zone-boundary spin-wave energy of $6J_0S$ (~ 75 meV) due to the octahedral coordination of the Fe sites. The average zone-boundary spin-wave energy for YBaFe$_2$O$_5$ (~ 60 meV) is very close to $5J_0S$. Therefore, the SWDOS in YBaFe$_2$O$_5$ is comparable to LaFeO$_3$, after accounting for the one broken AF exchange bond (five nearest neighbors) present in the square-pyramidal coordination.

While the comparison of the AF$_{CO}$ spectrum to that of LaFeO$_3$ shows that the energy scale of the SWDOS in YBaFe$_2$O$_5$ is set by the average exchange $\langle J \rangle \approx J_0$, details such as the appearance of split peaks (see Fig. 2) can be explained only by taking into account the variations in the exchange between different Fe-Fe pairs. As illustrated in Fig. 1(a), charge order in the AF$_{CO}$ phase consists of Fe^{2+} and Fe^{3+} chains along the *b* axis, resulting in four unique nearest-neighbor SE paths, given by J_{33}^b, J_{22}^b, J_{23}^a, and J_{23}^c, where the subscripts indicate the valences of the Fe-Fe pairs and the superscripts denote the direction of the magnetic bonds. It is reasonable to assume that the SE integral can be transferred from LaFeO$_3$ to the Fe^{3+}-Fe^{3+} pair in YBaFe$_2$O$_5$ using the relationship $J_{33}^b \propto (1/S^2)t^4 \cos^2\theta$ [11], where *t* is the Fe^{3+}-O transfer integral (for 180° bond angles) which depends sensitively on the Fe-O distance *d* as $t \propto d^{-7/2}$ [9] and θ is the Fe-O-Fe bond angle. We have used the resulting estimate for J_{33}^b (5.9 meV) as a starting point for studies of model calculations using the Heisenberg Hamiltonian

$$H = \sum_{\langle i,j \rangle} J_{ij} \mathbf{S}_i \cdot \mathbf{S}_j, \tag{2}$$

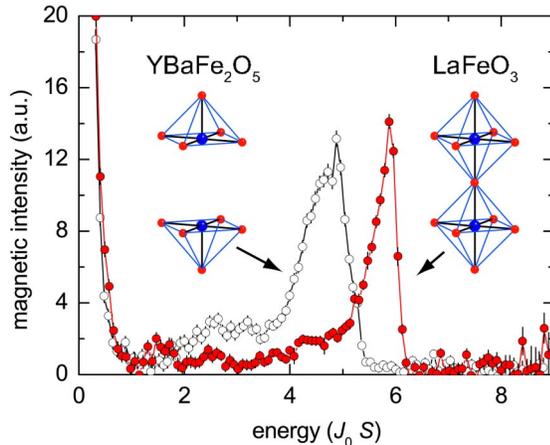where J_{ij} is the exchange energy between spins $\mathbf{S}_i$ and $\mathbf{S}_j$,

and $\langle i, j \rangle$ indicates that the sum is only over nearest neighbors. The Heisenberg Hamiltonian given in Eq. (2) was used within linear spin-wave theory to obtain spin-wave energies and eigenvectors from which neutron intensities due to coherent scattering $S(\mathbf{Q}, E)$ were calculated. For a more detailed discussion of model spin-wave calculations, see Ref. [12]. Polycrystalline averaging of $S(\mathbf{Q}, E)$ was performed by Monte Carlo integration over 10 000 **Q** vectors on each constant-*Q* sphere. The model calculations show that the two peak energies in YBaFe$_2$O$_5$ (at 58 and 62 meV) depend on

$$E_2 \approx 2J_{22}^b S_2 + (2J_{23}^a + J_{23}^c)S_3,$$
$$E_3 \approx 2J_{33}^b S_3 + (2J_{23}^a + J_{23}^c)S_2, \tag{3}$$

where S_i are 5/2 and 2 for Fe^{3+} or Fe^{2+}, respectively. These two energies are understood as the local excitation energy of the Fe^{3+} (Fe^{2+}) spin inside the respective square pyramid. The combination $J_{23} = (2J_{23}^a + J_{23}^c)/3$ shifts the center of mass of the entire spin-wave band, and J_{22}^b controls the splitting of the two peaks. Best agreement with both the splitting and the intensity ratio of the two peaks results in $J_{33}^b \approx 5.9$ meV, $J_{22}^b \approx 3.4$ meV, and $J_{23} \approx 6.0$ meV for the charge-ordered state AF$_{CO}$. The calculated powder-averaged magnetic neutron intensities $S(Q, E)$ and $S(E)$, shown in Figs. 2(b) and 2(c), respectively, are in excellent agreement with the measured data.

Figure 4 shows the magnetic intensity as a function of temperature from 6 to 450 K. Below $T_V = 308$ K, the main
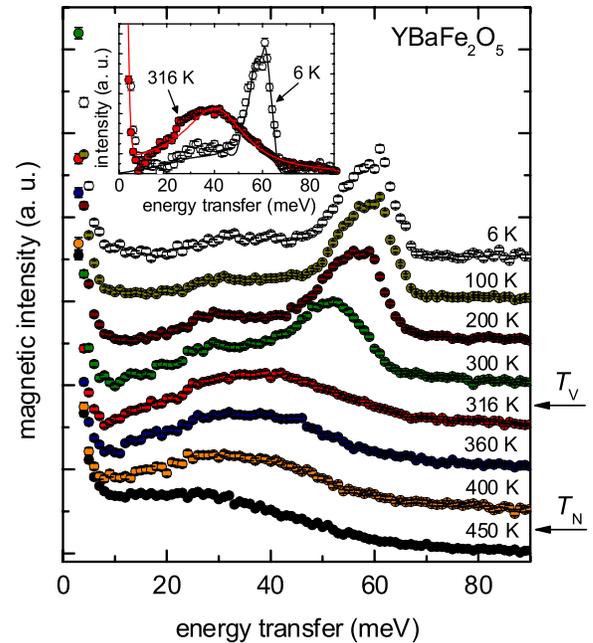

FIG. 3 (color online). Magnetic scattering intensity for YBaFe$_2$O$_5$ at 6 K and LaFeO$_3$ [10] at 10 K. Insets show idealized oxygen square pyramids (octahedra) in YBaFe$_2$O$_5$ (LaFeO$_3$) illustrating the broken magnetic bond in YBaFe$_2$O$_5$ in comparison to LaFeO$_3$.

FIG. 4 (color online). Temperature dependence of the magnetic scattering intensity for YBaFe$_2$O$_5$ between 6 and 450 K. Intensities at each temperature have been offset by a uniform amount for clarity. Spectra at 6 (AF$_{CO}$) and 316 K (AF$_{VM}$) are compared in the inset. The lines are results of a fit to a damped harmonic oscillator model (316 K data) and a Heisenberg model calculation (6 K data).

spin-wave band is at 60 meV, as discussed above, although there is some broadening and softening in energy at 300 K, just below T_V. At 316 K, just above T_V in the AF_{VM} phase, a dramatic shift in the energy of the spin-wave peak down to 40 meV is accompanied by a huge broadening of the spin-wave band. Above $T_N = 432$ K [6], paramagnetic scattering is observed. Spectra in the AF_{CO} and AF_{VM} phases are compared in the inset of Fig. 4. The large decrease of the zone-boundary spin-wave energy and the massive broadening in the valence-mixed AF_{VM} phase do not arise from normal SE interactions and cannot be reproduced by a simple Heisenberg model. The broadening may arise from a distribution of exchange along different paths and/or from the presence of overdamped modes. In the AF_{VM} phase, the valence-mixed Fe ions are electronically equivalent and occupy a single crystallographic site with Fe-O-Fe bond distances nearly identical in all directions. Thus, a decrease in the spin-wave bandwidth is expected in the AF_{VM} phase in comparison to AF_{CO}.

The flipping of the sign of the direct exchange from AF (AF_{CO}) to F (AF_{VM}) at T_V may be expected to have a significant effect on the SWDOS. However, introduction of the direct exchange J_{direct} to model spin-wave calculations leads to a splitting of the SWDOS proportional to J_{direct} rather than a decrease in energy of the entire spectrum. This confirms that J_{direct} does not have a significant effect on the SWDOS, as was already expected from Eq. (1). Therefore, the broadening and decrease in energy of the zone-boundary spin waves suggest damping arising from a strong coupling of spin excitations within double layers to valence-mixed charge carriers.

The large changes in the spin-wave spectrum at T_V are explained by the appearance of new ferromagnetic interactions within the double layers. Valence-mixed t_{2g} bands give rise to ferromagnetic DE that competes with e_g AF SE. In doped perovskite manganites, strong Hund's rule coupling of the itinerant e_g electron to the localized t_{2g} spin overwhelms the AF SE, leading to ferromagnetism via DE [13]. In other words, metallic ferromagnetism in the manganites is established in the limit $J_{DE} > J_{SE}$, where J_{DE} and J_{SE} represent DE and SE, respectively, within a Heisenberg model. To estimate the strength of the DE within double layers, the spin-wave spectrum at 316 K in AF_{VM} was fit using a damped harmonic oscillator model

$$S(E) = \frac{1}{1 - e^{-E/k_B T}} \frac{S_0 E \Gamma}{(E^2 - E_0^2)^2 + (E\Gamma)^2}, \quad (4)$$

where $(1 - e^{-E/k_B T})^{-1}$ is the Bose factor, $\Gamma = 33(1)$ meV is the width, and $E_0 = 45.8(4)$ meV is the position. The fit is shown in the inset in Fig. 4. We estimate the average exchange energy from $E_0 = 5\langle J \rangle S$, resulting in $\langle J \rangle \approx$ 4.07 meV, a 23% decrease from AF_{CO}. Given that the average exchange energy in the valence-mixed AF_{VM} phase of $YBaFe_2O_5$ is $\langle J \rangle = J_{SE} + J_{DE} \approx 4.07$ meV and $J_{SE} \approx 5.3$ meV in the charge-ordered AF_{CO} phase, we estimate that $J_{DE} \approx -1.2$ meV and $|J_{DE}/J_{SE}| \approx 0.23$. In

contrast to the manganites, conduction in $YBaFe_2O_5$ proceeds via the minority spin t_{2g} electron, whose spin must be opposite that of the local spin on the half-filled Fe^{3+} ion by the Pauli exclusion principle. Therefore, spin-polarized conduction within a double layer must overcome the AF structure established by the stronger, e_g-dominated SE. This can occur by flipping the spin on one Fe ion, momentarily creating an arrangement of five neighboring Fe spins that are ferromagnetically aligned with the central spin. It is then possible for real hopping of the t_{2g} electron to occur within a double layer through a DE-type process. Flipping the spin at one Fe site costs an energy of $5\langle J \rangle S^2 \approx 0.1$ eV. This scenario is consistent with conductivity measurements in $GdBaFe_2O_5$ [14], indicating that transport is an activated process in the valence-mixed phase, with an activation energy of about 0.1 eV. Such a hopping process will strongly disrupt near-neighbor spin correlations, leading to massive damping of zone-boundary spin waves. From the perspective of the zone-boundary spin waves, DE implies that deviations of the relative angle between neighboring spins makes electron hopping easier [2], causing the decay of the zone-boundary spin wave into charge and multimagnon excitations. Given such a picture, a significant change in the activation energy should be observed in resistivity in applied magnetic fields or at T_N.

*schang@ameslab.gov
[1] C. Zener, Phys. Rev. **82**, 403 (1951).
[2] Y. Tokura, Rep. Prog. Phys. **69**, 797 (2006).
[3] P. Karen, J. Solid State Chem. **177**, 281 (2004).
[4] P. M. Woodward and P. Karen, Inorg. Chem. **42**, 1121 (2003).
[5] P. Karen *et al.*, Phys. Rev. B **64**, 214405 (2001).
[6] P. M. Woodward, E. Suard, and P. Karen, J. Am. Chem. Soc. **125**, 8889 (2003).
[7] P. W. Anderson, Phys. Rev. **115**, 2 (1959); J. B. Goodenough, *ibid.* **171**, 466 (1968).
[8] T. Mizokawa and A. Fujimori, Phys. Rev. Lett. **80**, 1320 (1998); A. E. Bocquet *et al.*, Phys. Rev. B **45**, 1561 (1992).
[9] W. A. Harrison, *Electronic Structure and the Properties of Solids* (Dover, New York, 1989).
[10] R. J. McQueeney *et al.*, Phys. Rev. Lett. **98**, 126402 (2007).
[11] S. K. Mishra and S. Satpathy, Phys. Rev. B **58**, 7585 (1998); H. Meskine, H. König, and S. Satpathy, *ibid.* **64**, 094433 (2001).
[12] R. J. McQueeney *et al.*, Phys. Rev. B **73**, 174409 (2006).
[13] J. van den Brink and D. Khomskii, Phys. Rev. Lett. **82**, 1016 (1999).
[14] J. Lindén *et al.*, Phys. Rev. B **73**, 064415 (2006).